DR. MICHELE PORCU (Orcid ID : 0000-0002-3090-8541)

Article type : Research Report

The influence of the volumetric composition of the intracranial space on neural activity in healthy subjects: a resting-state functional magnetic resonance study.

The influence of the VOCICS on neural activity.

Authors: Michele Porcu[1], Max Wintermark[2], Jasjit S. Suri[3], Luca Saba[1]

[1]Department of Medical Imaging, AOU of Cagliari, University of Cagliari, Italy

[2]Department of Radiology, Neuroradiology Division, Stanford University, Stanford, California, USA

[3]Diagnostic and Monitoring Division, AtheroPoint, Roseville, California, USA

This article has been accepted for publication and undergone full peer review but has not been through the copyediting, typesetting, pagination and proofreading process, which may lead to differences between this version and the Version of Record. Please cite this article as doi: 10.1111/EJN.14627

Corresponding author: Michele Porcu (e-mail: micheleporcu87@gmail.com / institutional mail: m.porcu@aoucagliari.it) Department of Medical Imaging, Azienda Ospedaliera Universitaria di Cagliari – S.S. 554, km 4.500 – CAP: 09042 – Monserrato (Cagliari, Italy)

- Proposed Journal section: Clinical and Translational Neuroscience
- Total number of pages: 23
- Total number of figures: 5
- Total number of tables: 7
- Total number of words (whole manuscript): 4099
- Total number of words (abstract): 163
- Keywords: Volumetric composition of the intracranial space; resting state functional connectivity magnetic resonance; fALFF; graph theory.

Abstract

Brain atrophy is a condition observed both with healthy aging and in association with neurologic pathological conditions. We investigated the role of the volumetric composition of the intracranial space (VOCICS) in terms of relative brain volume (BV%) and relative cerebrospinal fluid volume (CSFV%) on the neural activity measured by resting-state functional Magnetic Resonance Imaging (rs-fMRI). We performed a group rs-fMRI analysis of a dataset of 192 healthy subjects derived by the publicly available Functional Connectome Project. Automatic volumetric analysis of structural data was performed in order to obtain BV% and CSFV% for every subject. Two fractional Amplitude of Low Frequency Fluctuations (fALFF) and two Region of interest to Region of interest (ROI-to-ROI) analyses were then performed using BV% and CSFV% as second level covariates, adopting a multiple regression statistic test in order to evaluate the effects of BV% and CSFV% on brain networks. The analyses revealed that VOCICS broadly influence brain networks. In conclusion, VOCICS significantly influences brain activity measured by rs-fMRI, and this parameter could represent an easy marker of brain connectivity in healthy young subjects.

Introduction

Resting state functional magnetic resonance imaging (rs-fMRI) is a widely used imaging technique for the study of normal and pathological brain activity (*Lv et al., 2018*). It was described for the first time in 1995 by *Biswal et al.* in 1995 (Biswal et al., 1995). It leverages the changes of blood-oxygen level-dependent (BOLD) signal generated by both oxygen consumption and microvascular reactivity during spontaneous neuronal activity (Buchbinder, 2016; Nasrallah et al., 2015). There are different accepted methods of analysis described in literature (*Lv et al., 2018*).

Brain morphometry is another technique of analysis broadly used in neuroscience for the study and quantification of anatomical features of individual brains or brains in populations (*Mietchen & Gaser, 2009*) Several algorithms and techniques have been developed for this analysis (*Gao et al., 2014*).

Because the brain is a complex system, and because a number of physiological and pathological mechanisms still remain unknown or incompletely understood, different neuroimaging datasets have been made available that can be freely analyzed by scientists all over the world in order to better analyze and understand this complex system; two examples are represented by the OpenfMRI (*Poldrack & Gorgolewski, 2015*) and the Consortium for Reliability and Reproducibility (*Zuo et al., 2014*) projects.

A recent interesting paper by *Qing Z et al.* (*Qing & Gong, 2016*) investigated the influence of brain volume on the rs-fMRI results in normal healthy young subjects. The authors found a robust linear correlation between brain volume and intrinsic brain activity measured by amplitude of low-frequency fluctuations (ALFF). This intriguing result of course opened a discussion on the influence of morphometric parameters on rs-fMRI in normal subjects.

The purpose of our research was to study the effects of the volumetric composition of the intracranial space (VOCICS) on rs-fMRI; VOCICS was expressed in terms of relative volumes of brain and cerebrospinal fluid compared to the intracranial volume. The neuroimaging dataset analyzed is part of the 1000 Functional Connectome Project (*Biswal et al., 2010*). In order to facilitate the lecture of the manuscript, all the abbreviations that are used in are reported in Table 1.

Materials and methods

Study design and ethical approval

The study was designed as post-hoc data analysis. No ethical approval was required due to the fact that the analyzed data was made publicly available by the 1000 Functional Connectome Project (*Biswal et al., 2010*).

Subjects and Imaging acquisitions

We analyzed a subset of the neuroimaging dataset of the *1000 Functional Connectome Project*, publicly available at www.nitrc.org/projects/fcon_1000/ (*Biswal et al., 2010*). The subset analyzed was the "Beijing_Zang" (*Tian et al., 2011; Chao-Gan & Yu-Feng, 2010*): it consisted of neuroimaging data of 192 right-handed normal young healthy subjects with (74 males: mean age 21.20 $\pm$ 1.76, range 18-26; 118 females: mean age 21.18 $\pm$ 1.84, range 18-26). All the MRI scans were acquired at the imaging center for Brain Research of the Beijing Normal University, using a Siemens TRIO 3.0 Tesla scanner (Siemens®, Erlangen, Germany). For every single patient two sequences were acquired: a) a structural T1-weighted sagittal three-dimensional magnetization-prepared rapid gradient echo (T1-MPRAGE), covering the entire brain: 128 slices, TR = 2530 ms, TE = 3.39 ms, slice thickness = 1.33 mm, flip angle = 7º, inversion time = 1100 ms, FOV = 256 × 256 mm, and in plane resolution = 256 × 192; b) a resting state BOLD echo-planar imaging (EPI) sequence, with closed eyes, and the following parameters: 33 axial slices, thickness: 3 mm, gap: 0.6 mm, in-plane resolution = 64 x 64, TR = 2000 ms, TE = 30 ms, flip-angle = 90°, FOV = 200 x 200 mm, slice acquisition order: interleaved ascending.

Morphometric analysis

The structural T1-MPRAGE sequences of all the 192 patients were evaluated by two expert neuroradiologists (MP and LS, 7 years and 14 years of radiological experience in neuroimaging respectively), in order to exclude the presence of pathological/anatomical abnormalities (included the presence of cortical dysplasia and/or abnormalities of the ventricular system and subarachnoid cisterns) and of gross movement artifacts. None of these findings was

found in the datasets assessed and therefore none was excluded from the morphometric analysis.

The morphometric analysis was performed using the VolBrain tool (*Manjón & Coupé, 2016*), an automated voxel-based MRI brain volumetry system. All the data derived from the morphometric analysis was checked by the same two neuroradiologists who evaluated the T1-MPRAGE sequences. They visually checked the volumetric inclusion of the brain tissues and CSF spaces in order to exclude anomalous segmentations performed with the automated algorithm; no critical findings were found, and no patients were excluded from the sub-sequent phases study. For each patient, the intracranial volume (ICV), brain volume (BV; the total brain tissue inside the intracranial space), and the CSF volume (CSFV; the total amount of CSF inside the intracranial space, localized in ventricular system and subarachnoid spaces) were quantified in cm^3; the relative volume of both BV and CSF expressed as percentage values was calculated using the following ratios: 1) BV / ICV ratio (BV%), and 2) CSFV / ICV ratio (CSFV%).

In order to assess the normal distribution of the population in terms of age, BV% and CSF% the Lillefors corrected Kolmogorov-Smirnov test was performed by using the IBM® SPSS® version 24.0 (IBM®, Armonk, NY, USA).

Rs-fMRI analysis

The rs-fMRI analysis was performed by using the CONN-fMRI fc toolbox v17b (*Whitfield-Gabrieli & Nieto-Castanon, 2012*) and SPM 12 (Wellcome Department of Imaging Neuroscience, London, UK; http://www.fil.ion.ucl.ac.uk/spm/) on MATLAB R2017b platform (MathWorks®, Natick, MA, USA). The CONN toolbox can perform seed-based correlation analysis evaluating the low-frequency temporal fluctuations of the BOLD signal. All the structural T1-MPRAGE sequences and functional EPI sequences were pre-processed using the CONN's default pipeline for volume-based analysis (except spatial smoothing), according to these steps:

a) functional realignment and unwarping
b) functional centering to (0,0,0) coordinates
c) functional slice-timing correction

d) functional outlier detection using intermediate settings (97th percentile in normative sample in functional outlier detection system, with Global-signal z-value threshold = 5 and Subject-motion mm threshold = 0.9)
e) functional direct simultaneous segmentation of grey matter, white matter and CSF, and normalization to Montreal Neurological Institute (MNI) space adopting default Tissue Probability Maps (target resolution = 2 mm)
f) structural centering to (0,0,0) coordinates;
g) structural simultaneous segmentation of grey matter, white matter and CSF, and normalization to MNI space by using the default Tissue Probability Maps (target resolution = 2 mm)

As suggested by *Alakörkkö T et al.* (*Alakörkkö T et al., 2017*), spatial smoothing was not performed in order to avoid to artificially influence the network properties, in particular degrees and centrality measures of the functional networks nodes.

BOLD signal registered in ventricular system and cerebral white matter were removed by using the principal component analysis of multivariate BOLD signal within each one of these masks; a denoising process was then applied to the BOLD data with a default band-pass filter (0.008 to 0.09 Hz) in order to reduce both noise effects and low frequency drift (*Porcu et al, 2019; Flodin et al., 2014*).

Two different second-level analyses were then performed: a) a voxel to voxel group analysis that evaluated the fractional amplitude of low frequency fluctuations (fALFF) normalized index (*LV et al., 2018; Zou et al., 2008*) and b) a regions of interest to region of interest (ROI-to-ROI) analysis (*Lv et al., 2018*). The CONN's default atlas was used for the definition of regions of interest (ROIs) in the ROI-to-ROI analysis, and for the anatomic localization of voxels in the fALFF analysis: cortical and subcortical ROIs derived from the Harvard-Oxford atlas (*Makris et al., 2006; Frazier et al., 2005; Desikan et al., 2006; Goldstein et al., 2007*), and cerebellar ROIs from the Automated Anatomical Labelling (AAL) atlas (*Tzourio-Mazoyer et al., 2002*).

fALFF computes for each voxel the relative amplitude (root mean square ratio) of BOLD signal fluctuations in the frequency band of interest (previously selected in the denoising process - 0.008 to 0.09 Hz) compared to the entire frequency band (before filtering) and is proportional to regional neural activity (*Lv et al., 2018*). Two different fALFF multiple regression analyses were

conducted including all subjects (value "0" assigned to every subject), with BV% and CSFV% as second level covariates: the first one (Analysis 1A) focused on the individual effects of BV%, and the second one (Analysis 2A) on the individual effects of CSFV%. In order to identify statistically significant results, a default peak p-value uncorrected (peak p-unc) < 0.001 was chosen as height threshold, and a default cluster-size p-value corrected for false discovery rate (cluster-size p-FDR) < 0.05 was adopted for cluster threshold (*Roiser et al., 2016; Chumbley & Friston, 2009*). Parametric statistics was adopted for both analyses: it exploits parametric distributions (Random Field Theory (*Worsley et al., 2004*)) for cluster-level statistics (*Chumbley et al., 2010*). One-sided negative, one-sided positive and two-sided analysis results directionality were applied for both analyses.

ROI-to-ROI functional connectivity is able to identify regions correlated with the activity in a seed region (*Lv et al., 2018*). Individual correlation maps of the whole brain were generated exploiting the mean resting-state BOLD signal time course from each ROI and then calculating the correlation coefficients with the BOLD signal time-course between ROIs. Correlations were derived by applying the General Linear Model (GLM) and bivariate correlation analysis weighted for Haemodynamic Response Function (HRF): higher Z-scores reflected positive correlations between ROIs, and so increased functional connectivity reflected by increased BOLD signal time series synchronization; on the contrary, lower Z-scores were associated with negative correlations, i.e. reduced connectivity reflected by decreased synchronicity between ROIs. Fisher's transformation was applied to all Z-scores. Finally, correlation coefficients were converted into standard scores. The group connectivity analysis, as well as the fALFF, was performed using BV% and CSFV% as second level covariates. Two different multiple regression analyses were conducted: the first one (Analysis 1B) focused on the individual effects of BV% on brain connectivity, and the second one (Analysis 2B) on the individual effects of CSFV%. Results were displayed using graph theory (*Bullmore & Sporns, 2009; Bassett DS et al., 2018; Alexander-Bloch et al., 2013*), considering the ROIs as nodes of the network. For every ROI, degree, average path length, clustering coefficient, global efficiency, local efficiency, and betweenness centrality were calculated adopting a conventional two-sided p-value corrected for False Discovery Rate (p-FDR) < 0.05 in order to identify statistically significant correlations between ROIs, and a two-

sided cost value = 0.15 as adjacency matrix threshold for network edges (*Andrews-Hanna et al., 2014*).

Results

Demographic analysis

The summary of the demographic data and the results of the morphometric analysis are reported in Table 2 (Please refer to Table 2B in supporting document for complete data). The normal distribution of the population in terms of age, BV% and CSFV% was confirmed by the Lillefors corrected Kolmogorov-Smirnov test (age: p-value = < 0.0001; BV% and CSFV%: p-value = 0.021) (Table 3 and Figure 1).

fALFF analyses

Analysis 1A focused BV%, and Analysis 1B focused on CSFV%. Both the two analyses revealed that both BV% and CSFV% affect regional neural activity measured by fALFF, albeit in a different manner (Figure 2).

Analysis 1A (Figure 3 and 4) revealed that there is a statistically significant correlation between BV% and the regional activity of different areas of the brain measured with fALFF (Table 4, and Table 4B in supporting document for complete data): in particular when two-contrast was adopted, the analysis identified 353 clusters of voxel (size: 4 - 3427 voxels; minimum T value = 3.34; cluster-size p-FDR: <0.000001 - 0.048277; peak p-unc: <0.000001 - 0.000144); when positive contrast was adopted, it found 57 clusters of voxel (size: 6 - 1444 voxels; minimum T value = 3.13; cluster-size p-FDR: <0.000001 - 0.045133; peak p-unc: <0.000001 - 0.000144); when negative contrast was adopted, it found 173 clusters of voxel (size: 6 - 2425 voxels; minimum T value = 3.13; cluster-size p-FDR: <0.000001 - 0.039978; peak p-unc: <0.000001 - 0.000351).

Analysis 1B revealed less statistically significant correlation between CSFV% and regional neural activity in terms of absolute numbers (Table 5): in particular when two-contrast was adopted, the analysis identified 4 clusters of voxel (size: 9 - 15 voxels; minimum T value = 3.34; cluster-size p-FDR: 0.007172 - 0.039153; peak p-unc: 0.000003 - 0.000046); when positive contrast was adopted, it found 1 cluster of voxel (size: 17 voxels; minimum T value = 3.13;

cluster-size p-FDR = 0.009197; peak p-unc = 0.000001); when negative contrast was adopted it found 5 clusters of voxel (size: 13 – 27 voxels; minimum T value = 3.13; cluster-size p-FDR: 0.000292 - 0.012197; peak p-unc: 0.000001 - 0.00003).

ROI-to-ROI analyses

Analysis 2A focused BV%, and Analysis 2B focused on CSFV%. Both the two ROI-to-ROI analyses, expressed using the graph theory, revealed statistically significant correlations between BV% and CSFV% and brain networks (Figure 5). In Analysis 2A (Table 6, and Table 6B in supporting document for complete data) the graph theory revealed that BV% is correlated with increased values of global efficiency (T value: 3.26 – 36.58; p-unc: <0.000001 - 0.001328; p-FDR: <0.000001 - 0.001328), local efficiency (T value: 2.6 - 42.03; p-unc: <0.000001 - 0.01077; p-FDR: <0.000001 - 0.01077) and average path length (T value: 7.02 – 16.83; p-unc: <0.000001 - 0.01077; p-FDR: <0.000001 - 0.01077) of all the 132 ROIs included in the study; clustering coefficients increased in 131 ROIs (T value: 2.82 – 16.83; p-unc: <0.000001 - 0.005438; p-FDR: <0.000001 - 0.00548); degree results increased in 128 ROIs (T value: 2.58 – 10.82; p-unc: <0.000001 - 0.010525; p-FDR: <0.000001 - 0.010854); betweenness centrality increased in 109 ROIs (T value: 2.09 – 6.06; p-unc: <0.000001 - 0.038166; p-FDR: 0.000001 - 0.04622).

In Analysis 2B (Table 7, and Table 7B in supporting document for complete data), average path lengths increased in 98 ROIs (T value: 2.11 – 6.15 ; p-unc: <0.000001 - 0.036281; p-FDR: 0.000001 - 0.048868); global efficiency increased in 89 ROIs showed and decreased in right and left 9th cerebellar lobule (T value: -2.77 – 5.58; p-unc: <0.000001 - 0.027173; p-FDR: 0.000007 - 0.039416); local efficiency was increased in 74 ROIs and reduced in left 7th cerebellar lobule (T value: -2.66 – 5.71; p-unc: <0.000001 - 0.028063; p-FDR: 0.000006 - 0.049391); clustering coefficients increased in 3 ROIs (T value: 3.42 – 4.06 ; p-unc: 0.000074 - 0.000772; p-FDR: 0.009737 - 0.033952); degree results increased only in anterior division of the right parahippocampal gyrus (T value = 3.85 ; p-unc = 0.000162; p-FDR = 0.021372); no ROIs showed statistically significant changes in betweenness centrality.

Discussion

In this study, we investigated the possible influence of the VOCICS on brain connectivity performing a seed free (fALFF) and a seed based (ROI-to-ROI with Graph theory) rsfMRI group analysis, adopting BV% and CSFV% (derived from automatic volumetric analysis) as second level covariates.

The quality and reliability of the data was verified by two expert neuroradiologists. The normal distribution of the population in terms of age, BV% and CSF% was confirmed by the Lillefors corrected Kolmogorov-Smirnov test.

As previously seen in the introductive section, the study by *Qing Z et al.* (*Qing & Gong, 2016*) showed a robust linear correlation between brain volume and intrinsic brain activity measured by ALFF, and the results of our research tend to confirm this observation, even if of course there are several methodological differences between our research and the aforementioned paper. First of all, it is important to underline that, in our study, we investigated the potential correlations between rs-fMRI and the relative volume of brain to IC (not the *absolute* volume), as well as relative volume of CSF to IC, expressed in percentage; we chose to analyze these two variables together due to their intrinsic linking by using a multiple regression statistic. Among the other differences, we chose fALFF method instead of ALFF due to its intrinsic higher specificity for grey matter (*Lv et al., 2018; Zou et al., 2008*), and further we performed a ROI-to-ROI analysis in order to investigate the influence of these parameters on the brain networks.

The comparison between fALFF analyses 1A and 1B clearly demonstrated that the regional neural activity is more influenced by BV% than by CSFV%. Analysis 1A also revealed that the neural activity varies differently in different regions of the brain: in particular, several areas within the Default Mode Network (DMN) (*Greicius et al., 2002*) showed increased regional activity correlated to the increment of the relative volume of the brain, including the principal hubs in both cerebral hemispheres (*Andrews-Hanna et al., 2014*): the posterior division of the cingulate gyrus, precuneus, the medial prefrontal cortex (that includes the anterior division of the cingulate gyrus, the paracingulate gyrus and the superior frontal gyrus), and angular gyrus on both sides. On the other hand, the same analysis showed other areas with reduced neural activity corelated with the increment of BV%, in particular the parahippocampal gyrus and the thalamus bilaterally, and the brain stem and the cerebellum infratentorially. As opposed to

Analysis 1A, very few statistically significant correlations were identified by Analysis 1B: the few supra-threshold voxels found to be negatively correlated with CSFV were located bilaterally within the superior frontal gyri, the caudate nuclei and the thalami.

ROI-to-ROI analyses 2A and 2B focused on the influence of BV% and CSFV% on brain networks. Degree (i.e. the number of connections for each ROI), average path length (i.e. average minimum path distance between each ROI and all other ROIs in the graph), clustering coefficient (i.e. the number of connections existing between the nearest neighbors of a ROI, expressed as proportion of the maximum number of possible links), global efficiency (i.e. average of inverse-distances between each ROI and all other ROIs in the graph, a measure of node centrality within a network), local efficiency (i.e. global efficiency of neighboring sub-graph, a measure of local integration related to clustering coefficient), and betweenness centrality (i.e. the fraction of all shortest paths in the network pass through a given ROI) were calculated for every ROI. In Analysis 2A, all the network measures were influenced by BV%: global efficiency, local efficiency and average path length values resulted increased in all the ROIs; betweenness centrality, clustering coefficient, and degree showed positive correlation with BV% in almost all the ROIs. Analysis 2A revealed that greater BV% value was associated with increased number of connections that link one ROI to the rest of the network as observed in degree measure, and a greater tendency to communicate one to each other and to organize in cluster as observed in clustering coefficient and betweenness centrality measures. Analysis 2B showed different results: global efficiency, local efficiency and average path length measures were influenced by CSFV% in more than 50% of all the ROIs, and in three ROIs resulted reduced (global efficiency of the 9th cerebellar lobules bilaterally, and local efficiency of the left 7th cerebellar lobule); clustering coefficients values resulted increased in only 3 ROIs, and degree value just in anterior division of the right parahippocampal gyrus. No statistically significant correlations were found between CSFV% and betweenness centrality. These results suggest a predominant (but not exclusive) role of BV% in terms of influencing brain networks.

The value of the present study is the demonstration of a relationship between neural activity and the VOCICS, i.e. BV% and CSFV%, in young healthy subjects. The lack of other similar studies on young healthy subjects (except the one by *Qing Z et al.* (*Qing & Gong, 2016*) that is the

only one that studied the correlation between brain volume and rs-fMRI to the best of our knowledge) do not allow us to draw definite conclusions that could explain these results.

The correlation between brain dimensions and brain function has always been a debated topic (*Qing & Gong, 2016; Rushton & Ankney, 2009*). It is known that aging is associated with brain atrophy and decline of cognitive function (*Nyberg et al., 2012; Aljondi et al., 2018; Morrison & Baxter, 2012*); further it has been established on rs-fMRI that aging is associated with posterior-to-anterior shift as an adaptive compensatory scaffolding mechanism (*Zhang H et al., 2017*), with reduced activity of the DMN (*Damoiseaux et al., 2008*) and increased in prefrontal nodes of the salience and fronto-parietal networks (*Witelson et al., 2006*). Less is known about the relationship between brain size and cognition/behavior and other cerebral functions in healthy subjects. For example, a research by research by *Nave et al.* (*Nave et al., 2019*) showed that there is a direct correlation between brain size and cognitive performances in healthy subjects, and another research by *Koppelmans V et al.* (*Koppelmans et al., 2017*) suggested a direct correlation between cerebellar volumes and motor and cognitive performances. Another example is a meta-analysis conducted by *Yuan P et al.* (*Yuan & Raz, 2014*) that studied the correlation between prefrontal cortex (PFC) volume and thickness with executive performances, confirming that larger PFC volume and greater PFC thickness were associated with better executive performance in healthy adults.

According to our results, we can then speculate that the VOCICS could influence also superior brain functions such as cognition and behavior, leading to new hypotheses. For example, according to Analysis 1A, it is reasonable to speculate that the reduced activity of the DMN associated with aging observed by *Damoiseaux JS et al.* (*Damoiseaux et al., 2008*) could be correlated in the general population with the reduction of BV% and the increase of CSFV% with age. We also observed that brains with greater values of BV% show brain networks with larger number of connections that link ROIs to each other and a greater tendency to organize in cluster. Based on this observation, it is conceivable that alterations of the brain networks seen on rs-fMRI in healthy aging (*Dennis & Thompson, 2014; Wiseman et al., 2017*) and in pathologies like Alzheimer disease and fronto-temporal dementia characterized by regional atrophy (*Risacher et al., 2017; Boccardi et al., 2003; delEtoile & Adeli, 2017; Reyes et al., 2018*) may be partly explained by differences in VOCICS.

We acknowledge two major limitations of our study. The first limitation is the lack of demographic and clinical data, in particular the ones pertaining to superior brain functions (for example cognition, behavior, motion function), limiting the correlation between VOCICS, superior brain functions, and neural activity and networks. The second limitation is the lack of comparison to another cohort of patients, similarly to *Qing Z et al.* (*Qing & Gong, 2016*). Because of the number of patients analyzed and the great number of statistically significant correlations found, it is reasonable to think that similar results would also be found in other and larger cohorts of patients. Further studies are needed to verify this hypothesis.

Conclusion

In conclusion, VOCICS could potentially represent an easy marker of brain connectivity in healthy young subjects, but more studies are necessary to analyze the correlations and implications between this parameter and superior brain functions. Further studies are needed to understand if these results can be generalized also in sub-groups of different demographic composition and sub-classes of pathologies. Further analysis would be important in order to understand if VOCICS also influences superior brain functions such as cognition and behavior.

Acknowledgments

M.P. thanks Dr. Paolo Siotto, Dr. Kimmo Mattila and Prof. Carsten Thomsen for their precious support in radiological education.

This research did not receive any specific grant from funding agencies in the public, commercial, or non-profit sectors.

Author contributions

Conceptualization, Michele Porcu and Luca Saba.; Methodology, Michele Porcu; Validation, Michele Porcu; Data Curation, Michele Porcu ; Investigation, M.P.; Writing – Original Draft, Michele Porcu ; Writing – Review and Editing, Luca Saba, Max Wintermark and Jasjit S. Suri; Supervision, Luca Saba and Max Wintermark.

Declaration of Interests

The authors declare no competing interests.

Data accessibility

Due to the large size of our project data (> 300 Gigabytes), all the data derived from volumetric analysis and the rs-fMRI elaborations are available through direct request to the corresponding author.

List of abbreviations

a) ALFF = Amplitude of Low Frequency Fluctuations
b) BOLD = Blood-oxygen level-dependent
c) BV = brain volume
d) BV% = relative brain volume
e) Cluster-size p-FDR = Cluster-size p-value corrected for false discovery rate

f) CSF = cerebrospinal fluid
g) CSFV = Cerebrospinal fluid volume
h) CSFV% = relative cerebrospinal fluid
i) DMN = Default Mode Network
j) EPI = Echo planar Imaging
k) fALFF = fractional Amplitude of Low Frequency Fluctuations
l) GLM = General linear model
m) HRF = Hemodynamic Response Function
n) ICV = Intracranial volume
o) P-FDR = p-value corrected for False Discovery Rate
p) Peak p-unc = Peak p-value uncorrected
q) ROI = Region of interest
r) ROI-to-ROI = Region of interest to Region of interest
s) rs-fMRI = resting state functional Magnetic Resonance Imaging
t) T1-MPRAGE = T1-weighted sagittal three-dimensional magnetization-prepared rapid gradient echo
u) VOCICS = volumetric composition of the intracranial space

Figure legends:

- **Figure 1**: Normal quantile-quantile (Q-Q) plots of age, BV% and CSFV% derived from the Lillefors corrected Kolmogorov-Smirnov tests. The normal distribution is confirmed for age (A), BV% (b) and CSFV% (C).
- **Figure 2**: Analysis 1A (on the left) and 1B (on the right). Maximum Intensity Projection (MIP) view of suprathreshold voxels: clusters of voxels that show increased regional neural activity are reddish colored, those with reduced activity are blueish colored. It is evident that BV% influences regional neural activity more than CSFV%.
- **Figure 3**: Analysis 1A. The picture shows clusters of increased (reddish colored) and reduced (blueish colored) regional neural activity correlated to BV% on individual slices on the three plane (axial, sagittal and coronal – neurological orientation). It is evident the direct correlation (increased activity) between BV% and neural activity of several areas of the brain, in particular within the DMN in precuneus, posterior and anterior division of the cingulate gyrus and medial prefrontal cortex; it is also evident that BV% value is inversely correlated (reduced activity) with the neural activity of other areas of the brain, included brainstem and cerebellum.
- **Figure 4**: Analysis 1A. A simplified virtual representation that shows on a three dimensional model the areas of increased (reddish colored) and reduced (blueish colored) regional neural activity correlated to BV%.
- **Figure 5**: Analysis 2A (on the top) and 2B (on the bottom). Results are exposed using the graph theory. Degree, average path length, clustering coefficient, global efficiency, local efficiency and betweenness centrality of the single ROIs were measured in both the cases, and it is evident that both BV% and CSFV% influence brain networks properties, even if in a different manner.

Tables legends:

- **Table 1**: List of abbreviations and the list of the analyses conducted.
- **Table 2**: Demographic and morphometric data. IC = intracranial; CSF = cerebrospinal fluid; BV% = brain volume / intracranial volume ratio (expressed in percentage); CSFV% = CSF volume / intracranial volume ratio (expressed in percentage). ICV, brain volume and CSF volume are expressed in cm3. Complete demographic data are reported Supporting document - Table 2B.
- **Table 3**: Results derived by the the Lillefors corrected Kolmogorov-Smirnov test. dof = degree of freedom; BV% = brain volume / intracranial volume ratio; CSFV% = cerebrospinal fluid volume / intracranial volume ratio.
- **Table 4**: Analysis 1A: results and relative statistics. In the right column are reported results when the two-sided contrast was adopted, in the middle column those derived by the adoption of one-sided positive contrast, and on the left column those derived by the adoption of one-sided negative contrast. On the top of the table the 20 biggest clusters identified by the analysis are reported: their peak-voxel location within each cluster on the MNI space (Clusters x,y,z), their size, and the relative statistics are reported. On the bottom of the table the main belonging groups of all the suprathreshold voxels identified in the analysis are reported. Size-p-FWE = cluster-size p-value corrected for Family-Wise Error; size-p-FDR = cluster-size p-value corrected for False Discovery Rate; size p-unc = cluster-size p-value uncorrected; peak p-FWE = peak-voxel p-value corrected for Family Wise Error; peak p-unc = peak-voxel p-value uncorrected; T(190)_min = minimum T value; k_min = minimum number of voxels (*Chumbley et al., 2010*). Complete data are reported in supporting document - Table 4B.
- **Table 5**: Analysis 1B: results and relative statistics. In the right column are reported results when the two-sided contrast was adopted, in the middle column those derived by the adoption of one-sided positive contrast, and on the left column those derived by the adoption of one-sided negative contrast. On the top of the table the clusters identified by the analysis are reported: their peak-voxel location within each cluster on the MNI space (Clusters x,y,z), their size, and the

relative statistics are reported. On the bottom of the table the belonging groups of all the suprathreshold voxels identified in the analysis are reported. Size-p-FWE = cluster-size p-value corrected for Family-Wise Error; size-p-FDR = cluster-size p-value corrected for False Discovery Rate; size p-unc = cluster-size p-value uncorrected; peak p-FWE = peak-voxel p-value corrected for Family Wise Error; peak p-unc = peak-voxel p-value uncorrected; T(190)_min = minimum T value; k_min = minimum number of voxels (*Chumbley et al., 2010*).

- **Table 6**: Analysis 2A: results exposed using the graph theory and relative statistics. Degree, average oath length, clustering coefficient, global efficiency, local efficiency and betweenness centrality of the single ROIs are reported: for every one of these parameters, the twenty regions with the highest T-value are reported. ROI = Region of Interest; beta = beta value; T = T-value; dof = degree of freedom; p-unc = p-value uncorrected; p-FDR = p-value corrected for False Discovery Rate; FP r = Frontal Pole Right; FP l = Frontal Pole Left; IC r = Insular Cortex Right; IC l = Insular Cortex Left; SFG l = Superior Frontal Gyrus Left; MidFG r = Middle Frontal Gyrus Right; MidFG l = Middle Frontal Gyrus Left; IFG oper l = Inferior Frontal Gyrus, pars opercularis Left; PreCG r = Precentral Gyrus Right; PreCG l = Precentral Gyrus Left; TP r = Temporal Pole Right; TP l = Temporal Pole Left; aMTG r = Middle Temporal Gyrus, anterior division Right; aMTG l = Middle Temporal Gyrus, anterior division Left; pMTG r = Middle Temporal Gyrus, posterior division Right; pMTG l = Middle Temporal Gyrus, posterior division Left; PostCG r = Postcentral Gyrus Right; PostCG l = Postcentral Gyrus Left; SPL l = Superior Parietal Lobule Left; pSMG l = Supramarginal Gyrus, posterior division Left; AG r = Angular Gyrus Right; AG l = Angular Gyrus Left; sLOC l = Lateral Occipital Cortex, superior division Left; iLOC r = Lateral Occipital Cortex, inferior division Right; MedFC = Frontal Medial Cortex; FOrb l = Frontal Orbital Cortex Left; aPaHC r = Parahippocampal Gyrus, anterior division Right; LG r = Lingual Gyrus Right; LG l = Lingual Gyrus Left; CO r = Central Opercular Cortex Right; CO l = Central Opercular Cortex Left; PO r = Parietal Operculum Cortex Right; PP r = Planum Polare Right; PT r = Planum Temporale Right; PT l = Planum Temporale

Left; OP l = Occipital Pole Left; Brain-Stem = Brain Stem; Cereb1 r = Cerebelum Crus1 Right; Cereb2 l = Cerebelum Crus2 Left; Cereb2 r = Cerebelum Crus2 Right; Cereb6 l = Cerebelum 6 Left; Cereb6 r = Cerebelum 6 Right; Cereb9 l = Cerebelum 9 Left; Cereb9 r = Cerebelum 9 Right. Complete data are reported in supporting document - Table 6B.

- **Table 7**: Analysis 2B: results exposed using the graph theory and relative statistics. Degree, average oath length, clustering coefficient, global efficiency, local efficiency and betweenness centrality of the single ROIs are reported: for global efficiency, local efficiency and average path length, the twenty regions with the highest T-value are reported. ROI = Region of Interest; beta = beta value; T = T-value; dof = degree of freedom; p-unc = p-value uncorrected; p-FDR = p-value corrected for False Discovery Rate; FP r = Frontal Pole Right; FP l = Frontal Pole Left; IC r = Insular Cortex Right; IC l = Insular Cortex Left; SFG l = Superior Frontal Gyrus Left; MidFG r = Middle Frontal Gyrus Right; MidFG l = Middle Frontal Gyrus Left; IFG oper l = Inferior Frontal Gyrus, pars opercularis Left; PreCG r = Precentral Gyrus Right; PreCG l = Precentral Gyrus Left; TP r = Temporal Pole Right; TP l = Temporal Pole Left; aMTG r = Middle Temporal Gyrus, anterior division Right; aMTG l = Middle Temporal Gyrus, anterior division Left; pMTG r = Middle Temporal Gyrus, posterior division Right; pMTG l = Middle Temporal Gyrus, posterior division Left; aITG r = Inferior Temporal Gyrus, anterior division Right; toITG r = Inferior Temporal Gyrus, temporooccipital part Right; PostCG r = Postcentral Gyrus Right; AG r = Angular Gyrus Right; AG l = Angular Gyrus Left; sLOC l = Lateral Occipital Cortex, superior division Left; MedFC = Frontal Medial Cortex; SMA r = Juxtapositional Lobule Cortex -formerly Supplementary Motor Cortex- Right; PaCiG l = Paracingulate Gyrus Left; Precuneus = Precuneus Cortex; FOrb l = Frontal Orbital Cortex Left; aPaHC r = Parahippocampal Gyrus, anterior division Right; LG l = Lingual Gyrus Left; CO r = Central Opercular Cortex Right; CO l = Central Opercular Cortex Left; PO r = Parietal Operculum Cortex Right; PP r = Planum Polare Right; PT r = Planum Temporale Right; PT l = Planum Temporale Left; SCC l = Supracalcarine Cortex Left; Cereb2 l = Cerebelum Crus2 Left; Cereb7 r

= Cerebelum 7b Right; Cereb9 l = Cerebelum 9 Left; Cereb9 r = Cerebelum 9 Right; Ver45 = Vermis 4 5; Ver6 = Vermis 6. Complete data are reported in Supplemental material - Table 7B.

References:

- Alakörkkö T, Saarimäki H, Glerean E, Saramäki J, Korhonen O (2017) Effects of spatial smoothing on functional brain networks. Eur J Neurosci. 46(9):2471-2480.
- Alexander-Bloch A, Giedd JN, Bullmore E. (2013) Imaging structural co-variance between human brain regions. Nat Rev Neurosci. 14(5):322-36.
- Aljondi R, Szoeke C, Steward C, Yates P, Desmond P (2018) A decade of changes in brain volume and cognition. Brain Imaging Behav. doi: 10.1007/s11682-018-9887-z. [Epub ahead of print]
- Andrews-Hanna JR, Smallwood J, Spreng RN (2014) The default network and self-generated thought: component processes, dynamic control, and clinical relevance. Ann N Y Acad Sci. 1316(1):29-52.
- Bassett DS, Zurn P, Gold JI. (2018) On the nature and use of models in network neuroscience. Nat Rev Neurosci. 19(9):566-578.
- Biswal B, Yetkin FZ, Haughton VM, Hyde JS (1995) Functional connectivity in the motor cortex of resting human brain using echo-planar MRI. Magn Reson Med. 34:537–541.
- Biswal BB, Mennes M, Zuo XN, Gohel S, Kelly C, Smith SM, Beckmann CF, Adelstein JS, Buckner RL, Colcombe S et al. (2010) Toward discovery science of human brain function. Proc Natl Acad Sci U S A. 107(10):4734-9.
- Boccardi M, Laakso MP, Bresciani L, Galluzzi S, Geroldi C, Beltramello A, Soininen H, Frisoni GB (2003) The MRI pattern of frontal and temporal brain atrophy in fronto-temporal dementia. Neurobiol Aging. 24(1):95-103.
- Buchbinder BR (2016) Functional magnetic resonance imaging. Handb Clin Neurol. 135:61-92.
- Bullmore E, Sporns O (2009) Complex brain networks: graph theoretical analysis of structural and functional systems. Nat Rev Neurosci. 10(3):186-98.
- Chao-Gan Y, Yu-Feng Z (2010) DPARSF: A MATLAB Toolbox for "Pipeline" Data Analysis of Resting-State fMRI. Front Syst Neurosci. 4:13.
- Chumbley JR, Friston KJ (2009) False discovery rate revisited: FDR and topological inference using Gaussian random fields. Neuroimage.44(1):62-70
- Chumbley J, Worsley K, Flandin G, Friston K (2010) Topological FDR for neuroimaging. Neuroimage. 49(4):3057-64.
- Dalong G, Jiyuan L, Ying Z, Lei Z, Yanhong H, Yongcong S. (2018) Transcranial direct current stimulation reconstructs diminished thalamocortical connectivity during prolonged resting wakefulness: a resting-state fMRI pilot study. Brain Imaging Behav. doi: 10.1007/s11682-018-9979-9. [Epub ahead of print]
- Damoiseaux JS, Beckmann CF, Arigita EJ, Barkhof F, Scheltens P, Stam CJ, Smith SM, Rombouts SA (2008) Reduced resting-state brain activity in the "default network" in normal aging. Cereb Cortex. 18(8):1856-64.
- delEtoile J, Adeli H (2017) Graph Theory and Brain Connectivity in Alzheimer's Disease. Neuroscientist. 23(6):616-626.
- Dennis EL, Thompson PM (2014) Functional brain connectivity using fMRI in aging and Alzheimer's disease. Neuropsychol Rev.24(1):49-62.
- Desikan RS, SÈgonne F, Fischl B, Quinn BT, Dickerson BC, Blacker D, Buckner RL, Dale AM, Maguire RP, Hyman BT, et al. (2006) An automated labeling system for subdividing the human cerebral cortex on MRI scans into gyral based regions of interest. Neuroimage. 31(3):968-80

- Flodin P, Martinsen S, Löfgren M, Bileviciute-Ljungar I, Kosek E, Fransson P (2014) Fibromyalgia is associated with decreased connectivity between pain- and sensorimotor brain areas. Brain Connect. 4(8):587-94.
- Frazier JA, Chiu S, Breeze JL, Makris N, Lange N, Kennedy DN, Herbert MR, Bent EK, Koneru VK, Dieterich ME, et al. (2005) Structural brain magnetic resonance imaging of limbic and thalamic volumes in pediatric bipolar disorder. Am J Psychiatry. 162(7):1256-65.
- Gao Y, Riklin-Raviv T, Bouix S (2014) Shape analysis, a field in need of careful validation. Hum Brain Mapp. 35(10):4965-78.
- Goldstein JM, Seidman LJ, Makris N, Ahern T, O'Brien LM, Caviness VS Jr, Kennedy DN, Faraone SV, Tsuang MT (2007) Hypothalamic abnormalities in schizophrenia: sex effects and genetic vulnerability. Biol Psychiatry. 61(8):935-45.
- Greicius MD, Krasnow B, Reiss AL, Menon V (2002) Functional connectivity in the resting brain: a network analysis of the default mode hypothesis. Proc Natl Acad Sci U S A. 100(1):253-8.
- Koppelmans V, Hoogendam YY, Hirsiger S, Mérillat S, Jäncke L, Seidler RD (2017) Regional cerebellar volumetric correlates of manual motor and cognitive function. Brain Struct Funct. 222(4):1929-1944.
- Lv H, Wang Z, Tong E, Williams LM, Zaharchuk G, Zeineh M, Goldstein-Piekarski AN, Ball TM, Liao C, Wintermark M (2018) Resting-State Functional MRI: Everything That Nonexperts Have Always Wanted to Know. AJNR Am J Neuroradiol. 39(8):1390-1399.
- Makris N, Goldstein JM, Kennedy D, Hodge SM, Caviness VS, Faraone SV, Tsuang MT, Seidman LJ (2006) Decreased volume of left and total anterior insular lobule in schizophrenia. Schizophr Res. 83(2-3):155-71
- Manjón JV, Coupé P (2016) volBrain: An Online MRI Brain Volumetry System. Front Neuroinform. 10:30.
- Mietchen D, Gaser C. (2009) Computational morphometry for detecting changes in brain structure due to development, aging, learning, disease and evolution. Front Neuroinform. 3:25.
- Morrison JH, Baxter MG (2012) The ageing cortical synapse: hallmarks and implications for cognitive decline. Nat Rev Neurosci. 13(4):240-50.
- Nasrallah FA, Yeow LY, Biswal B, Chuang KH (2015) Dependence of BOLD signal fluctuation on arterial blood CO2 and O2: Implication for resting-state functional connectivity. Neuroimage. 117:29–39.
- Nave G, Jung WH, Karlsson Linnér R, Kable JW, Koellinger PD (2019) Are Bigger Brains Smarter? Evidence From a Large-Scale Preregistered Study. Psychol Sci. 30(1):43-54.
- Nyberg L, Lövdén M, Riklund K, Lindenberger U, Bäckman L (2012) Memory aging and brain maintenance. Trends Cogn Sci. 16(5):292-305.
- Poldrack RA, Gorgolewski KJ (2015) OpenfMRI: Open sharing of task fMRI data. Neuroimage. 144(Pt B):259-261.
- Porcu M, Craboledda D, Garofalo P, Barberini L, Sanfilippo R, Zaccagna F, Wintermark M, Montisci R, Saba L (2019) Reorganization of brain networks following carotid endarterectomy: an exploratory study using resting state functional connectivity with a focus on the changes in Default Mode Network connectivity. Eur J Radiol. 110:233-241.
- Qing Z, Gong G. (2016) Size matters to function: Brain volume correlates with intrinsic brain activity across healthy individuals. Neuroimage. 139:271-278.

- Reyes P, Ortega-Merchan MP, Rueda A, Uriza F, Santamaria-García H, Rojas-Serrano N, Rodriguez-Santos J, Velasco-Leon MC, Rodriguez-Parra JD, Mora-Diaz DE et al. (2018) Functional Connectivity Changes in Behavioral, Semantic, and Nonfluent Variants of Frontotemporal Dementia. Behav Neurol. 2018:9684129.
- Risacher SL, Anderson WH, Charil A, Castelluccio PF, Shcherbinin S, Saykin AJ, Schwarz AJ; Alzheimer's Disease Neuroimaging Initiative (2017) Alzheimer disease brain atrophy subtypes are associated with cognition and rate of decline. Neurology. 89(21):2176-2186.
- Roiser JP, Linden DE, Gorno-Tempinin ML, Moran RJ, Dickerson BC, Grafton ST (2016) Minimum statistical standards for submissions to Neuroimage: Clinical. Neuroimage Clin. 12:1045-1047.
- Rushton JP, Ankney CD (2009) Whole brain size and general mental ability: a review. Int J Neurosci. 119(5):691-731.
- Tian L, Wang J, Yan C, He Y. (2011) Hemisphere- and gender-related differences in small-world brain networks: a resting-state functional MRI study. Neuroimage. 54(1):191-202.
- Tzourio-Mazoyer N, Landeau B, Papathanassiou D, Crivello F, Etard O, Delcroix N, Mazoyer B, Joliot M (2002) Automated anatomical labeling of activations in SPM using a macroscopic anatomical parcellation of the MNI MRI single-subject brain. Neuroimage. 15(1):273-89
- Whitfield-Gabrieli S, Nieto-Castanon A (2012) Conn: a functional connectivity toolbox for correlated and anticorrelated brain networks. Brain Connect. 2(3):125-41.
- Wiseman SJ, Booth T, Ritchie SJ, Cox SR, Muñoz Maniega S, Valdés Hernández MDC, Dickie DA, Royle NA, Starr JM, Deary IJ et al. (2017) Cognitive abilities, brain white matter hyperintensity volume, and structural network connectivity in older age. Hum Brain Mapp. 39(2):622-632.
- Witelson SF, Beresh H, Kigar DL (2006) Intelligence and brain size in 100 postmortem brains: sex, lateralization and age factors. Brain. 129(Pt 2):386-98.
- Worsley KJ, Taylor JE, Tomaiuolo F, Lerch J (2004) Unified univariate and multivariate random field theory. Neuroimage. 23 Suppl 1:S189-95.
- Yuan P, Raz N (2014) Prefrontal cortex and executive functions in healthy adults: a meta-analysis of structural neuroimaging studies. Neurosci Biobehav Rev. 42:180-92.
- Zhang H, Lee A, Qiu A (2017) A posterior-to-anterior shift of brain functional dynamics in aging. Brain Struct Funct. 222(8):3665-3676.
- Zou QH, Zhu CZ, Yang Y, Zuo XN, Long XY, Cao QJ, Wang YF, Zang YF (2008) An improved approach to detection of amplitude of low-frequency fluctuation (ALFF) for resting-state fMRI: fractional ALFF. J Neurosci Methods. 172(1):137-41.
- Zuo XN, Anderson JS, Bellec P, Birn RM, Biswal BB, Blautzik J, Breitner JC, Buckner RL, Calhoun VD, Castellanos FX et al. (2014) An open science resource for establishing reliability and reproducibility in functional connectomics. Sci Data.1:140049.

List of abbreviations	
Terms	*Abbreviation*
Amplitude of low-frequency fluctuations	ALFF
Blood-oxygen level-dependent	BOLD
Brain Volume	BV
Relative brain volume	BV%
Cluster-size p-value corrected for false discovery rate	Cluster-size p-FDR
Cerebrospinal fluid	CSF
Cerebrospinal fluid volume	CSFV
Relative cerebrospinal fluid volume	CSFV%
Default Mode Network	DMN
Echo-planar imaging	EPI
Fractional amplitude of low-frequency fluctuations	fALFF
General Linear Model	GLM
Hemodynamic Response Function	HRF
Intracranial volume	ICV
p-value corrected for False Discovery Rate	p-FDR
Peak p-value uncorrected	Peak p-unc
Region of interest	ROI
Region of interest to Region of interest	ROI-to-ROI
Resting state functional magnetic resonance imaging	Rs-fMRI
T1-weighted sagittal three-dimensional magnetization-prepared rapid gradient echo	T1-MPRAGE
Volumetric composition of the intracranial space	VOCICS

List of the analyses	
Analysis 1A	fALFF analysis focused on BV%
Analysis 1B	fALFF analysis focused on CSFV%
Analysis 2A	ROI-to-ROI analysis focused on BV%
Analysis 2B	ROI-to-ROI analysis focused on CSFV%

Table 1: List of abbreviations and the list of the analyses conducted.

Demographic and morphometric data							
Subject	**Sex**	**Age**	**IC volume (cm3)**	**Brain volume (cm3)**	**CSF volume (cm3)**	**BV% (%)**	**CSF% (%)**
Mean values	**Males: 74 Females: 118**	**21.19**	**1465.1630**	**1300.4873**	**164.6757**	**88.8004**	**11.1995**

Table 2: Demographic and morphometric data. IC = intracranial; CSF = cerebrospinal fluid; BV% = brain volume / IC volume ratio (expressed in percentage); CSF% = CSF volume /IC volume ratio (expressed in percentage). IC volume, brain volume and CSF volume are expressed in cm^3. Complete demographic data are reported Supplemental material -Table 2B.

Test of Normality - Kolmogorov-Smirnov*			
	Statistic	**dof**	**p-value**
Age	0.183	192	< 0.001
BV%	0.071	192	0.021
CSFV%	0.071	192	0.021
***Lilliefors Significance Correction**			

Table 3: Results derived by the the Lillefors corrected Kolmogorov-Smirnov test. dof = degree of freedom; BV% = brain volume / intracranial volume ratio; CSFV% = cerebrospinal fluid volume / intracranial volume ratio.

Analysis 1A

Clusters - two sided contrast*

Cluster number	Clusters - x,y,z	size	size p-FWE	size p-FDR	size p-unc	peak p-FWE	peak p-unc
1	+00 -64 +28	3427	< 0.000001	< 0.000001	< 0.000001	< 0.000001	< 0.000001
2	+00 +46 +38	3376	< 0.000001	< 0.000001	< 0.000001	< 0.000001	< 0.000001
3	-16 -16 -46	1253	< 0.000001	< 0.000001	< 0.000001	0.002218	< 0.000001
4	+18 -18 +48	234	< 0.000001	< 0.000001	< 0.000001	0.019725	< 0.000001
5	-46 +20 -08	159	< 0.000001	< 0.000001	< 0.000001	0.003123	< 0.000001
6	-26 -18 +18	114	< 0.000001	< 0.000001	< 0.000001	0.029139	< 0.000001
7	+48 +22 -10	104	< 0.000001	< 0.000001	< 0.000001	0.01102	< 0.000001
8	-18 +16 +30	75	< 0.000001	< 0.000001	< 0.000001	0.133858	0.000001
9	-28 +12 +64	70	< 0.000001	< 0.000001	< 0.000001	0.007458	< 0.000001
10	+56 +12 +38	70	< 0.000001	< 0.000001	< 0.000001	0.049638	< 0.000001
11	+30 -14 +14	66	< 0.000001	< 0.000001	< 0.000001	0.247771	0.000001
12	-18 -24 +44	64	< 0.000001	< 0.000001	< 0.000001	0.003189	< 0.000001
13	-06 -30 -08	54	< 0.000001	< 0.000001	< 0.000001	0.097387	< 0.000001
14	+46 +50 -04	53	< 0.000001	< 0.000001	< 0.000001	0.001163	< 0.000001
15	-04 -14 -26	53	< 0.000001	< 0.000001	< 0.000001	0.434051	0.000002
16	-28 -52 -50	44	< 0.000001	< 0.000001	< 0.000001	0.020051	< 0.000001
17	-28 +04 +44	43	< 0.000001	< 0.000001	< 0.000001	0.997359	0.000005
18	-22 -18 -04	43	< 0.000001	< 0.000001	< 0.000001	0.038208	< 0.000001
19	+28 +00 +16	42	< 0.000001	< 0.000001	< 0.000001	0.067491	< 0.000001
20	-22 -44 +40	40	0.000001	< 0.000001	< 0.000001	0.145986	0.000001

Suprathreshold voxels

3801 voxels covering 1% of atlas.not-labeled

Clusters - positive contrast**

Cluster number	Clusters - x,y,z	size	size p-FWE	size p-FDR	size p-unc	peak p-FWE	peak p-unc
1	+00 -64 +28	4336	< 0.000001	< 0.000001	< 0.000001	< 0.000001	< 0.000001
2	+00 +46 +38	4258	< 0.000001	< 0.000001	< 0.000001	< 0.000001	< 0.000001
3	+56 +12 +38	217	< 0.000001	< 0.000001	< 0.000001	0.024819	< 0.000001
4	-46 +20 -08	217	< 0.000001	< 0.000001	< 0.000001	0.001562	< 0.000001
5	+48 +22 -10	134	< 0.000001	< 0.000001	< 0.000001	0.00551	< 0.000001
6	-28 +12 +64	133	< 0.000001	< 0.000001	< 0.000001	0.003729	< 0.000001
7	+46 +50 -04	74	< 0.000001	< 0.000001	< 0.000001	0.000581	< 0.000001
8	-08 -66 +24	69	< 0.000001	< 0.000001	< 0.000001	0.009104	< 0.000001
9	+28 +34 +52	54	< 0.000001	< 0.000001	< 0.000001	0.013814	< 0.000001
10	-24 +62 -06	44	0.000002	< 0.000001	< 0.000001	0.821799	0.000003
11	+00 -06 +64	43	0.000002	< 0.000001	< 0.000001	0.462322	0.000002
12	-48 -38 +58	41	0.000004	< 0.000001	< 0.000001	0.027257	< 0.000001
13	-26 +66 +00	37	0.000013	0.000001	< 0.000001	0.03443	< 0.000001
14	+12 +44 +52	36	0.000018	0.000001	< 0.000001	0.145758	0.000001
15	-58 -32 +52	36	0.000018	0.000001	< 0.000001	0.365101	0.000002
16	+56 -58 -04	31	0.000088	0.000007	< 0.000001	0.297068	0.000001
17	+22 +26 +62	24	0.000957	0.000067	0.000003	0.999999	0.000016
18	+26 +20 +62	23	0.001368	0.000086	0.000004	0.999987	0.000012
19	-40 +56 +02	23	0.001368	0.000086	0.000004	1	0.00004
20	+66 -22 +26	22	0.001967	0.000117	0.000006	0.351051	0.000001

Suprathreshold voxels

1444 voxels covering 26% of atlas.Precuneous (Precuneous Cortex)

Clusters - negative contrast***

Cluster number	Clusters - x,y,z	size	size p-FWE	size p-FDR	size p-unc	peak p-FWE	peak p-unc
1	-16 -16 -46	2425	< 0.000001	< 0.000001	< 0.000001	0.001109	< 0.000001
2	+24 -32 +48	663	< 0.000001	< 0.000001	< 0.000001	0.001475	< 0.000001
3	-18 -24 +44	317	< 0.000001	< 0.000001	< 0.000001	0.001594	< 0.000001
4	-26 -18 +18	163	< 0.000001	< 0.000001	< 0.000001	0.014569	< 0.000001
5	-34 -12 -14	122	< 0.000001	< 0.000001	< 0.000001	0.010165	< 0.000001
6	-18 +16 +30	95	< 0.000001	< 0.000001	< 0.000001	0.066929	< 0.000001
7	+16 -20 -02	78	< 0.000001	< 0.000001	< 0.000001	0.062426	< 0.000001
8	-22 -18 -04	76	< 0.000001	< 0.000001	< 0.000001	0.019104	< 0.000001
9	-36 -26 +34	74	< 0.000001	< 0.000001	< 0.000001	0.270942	0.000001
10	+34 +00 -28	69	< 0.000001	< 0.000001	< 0.000001	0.271648	0.000001
11	-28 -52 -50	69	< 0.000001	< 0.000001	< 0.000001	0.010025	< 0.000001
12	-36 -32 +08	65	< 0.000001	< 0.000001	< 0.000001	0.013735	< 0.000001
13	+40 -32 +00	64	< 0.000001	< 0.000001	< 0.000001	0.934357	0.000004
14	+16 +26 +34	60	< 0.000001	< 0.000001	< 0.000001	0.005415	< 0.000001
15	-22 -44 +40	59	< 0.000001	< 0.000001	< 0.000001	0.072993	< 0.000001
16	-52 -22 -38	59	< 0.000001	< 0.000001	< 0.000001	0.489899	0.000002
17	-14 -60 -44	52	< 0.000001	< 0.000001	< 0.000001	0.484376	0.000002
18	+38 -22 +34	51	< 0.000001	< 0.000001	< 0.000001	0.021916	< 0.000001
19	-22 -26 -26	50	< 0.000001	< 0.000001	< 0.000001	0.005948	< 0.000001
20	-48 -16 -22	44	0.000002	< 0.000001	< 0.000001	0.999995	0.000014

Suprathreshold voxels

4015 voxels covering 1% of atlas.not-labeled

1221 voxels covering 22% of atlas.Precuneous (Precuneous Cortex)	1145 voxels covering 0% of atlas.not-labeled	906 voxels covering 22% of atlas.Brain-Stem
830 voxels covering 10% of atlas.FP r (Frontal Pole Right)	1055 voxels covering 13% of atlas.FP r (Frontal Pole Right)	215 voxels covering 9% of atlas.Cereb8 r (Cerebelum 8 Right)
685 voxels covering 10% of atlas.FP l (Frontal Pole Left)	877 voxels covering 13% of atlas.FP l (Frontal Pole Left)	96 voxels covering 5% of atlas.Cereb8 l (Cerebelum 8 Left)
671 voxels covering 16% of atlas.Brain-Stem	825 voxels covering 17% of atlas.sLOC l (Lateral Occipital Cortex, superior division Left)	56 voxels covering 9% of atlas.aPaHC r (Parahippocampal Gyrus, anterior division Right)
642 voxels covering 13% of atlas.sLOC l (Lateral Occipital Cortex, superior division Left)	544 voxels covering 11% of atlas.sLOC r (Lateral Occipital Cortex, superior division Right)	54 voxels covering 4% of atlas.Thalamus l
438 voxels covering 18% of atlas.PC (Cingulate Gyrus, posterior division)	520 voxels covering 22% of atlas.PC (Cingulate Gyrus, posterior division)	53 voxels covering 6% of atlas.Cereb45 l (Cerebelum 4 5 Left)
426 voxels covering 9% of atlas.sLOC r (Lateral Occipital Cortex, superior division Right)	422 voxels covering 14% of atlas.MidFG l (Middle Frontal Gyrus Left)	51 voxels covering 7% of atlas.pTFusC r (Temporal Fusiform Cortex, posterior division Right)
338 voxels covering 12% of atlas.MidFG l (Middle Frontal Gyrus Left)	346 voxels covering 13% of atlas.AC (Cingulate Gyrus, anterior division)	48 voxels covering 8% of atlas.Cereb45 r (Cerebelum 4 5 Right)
311 voxels covering 12% of atlas.AC (Cingulate Gyrus, anterior division)	305 voxels covering 11% of atlas.SFG r (Superior Frontal Gyrus Right)	46 voxels covering 5% of atlas.pITG l (Inferior Temporal Gyrus, posterior division Left)
255 voxels covering 10% of atlas.SFG r (Superior Frontal Gyrus Right)	253 voxels covering 17% of atlas.AG r (Angular Gyrus Right)	46 voxels covering 5% of atlas.pTFusC l (Temporal Fusiform Cortex, posterior division Left)
202 voxels covering 14% of atlas.AG r (Angular Gyrus Right)	244 voxels covering 9% of atlas.SFG l (Superior Frontal Gyrus Left)	44 voxels covering 5% of atlas.Cereb9 l (Cerebelum 9 Left)
195 voxels covering 7% of atlas.SFG l (Superior Frontal Gyrus Left)	217 voxels covering 16% of atlas.PaCiG r (Paracingulate Gyrus Right)	44 voxels covering 6% of atlas.Cereb9 r (Cerebelum 9 Right)
188 voxels covering 14% of atlas.PaCiG r (Paracingulate Gyrus Right)	214 voxels covering 22% of atlas.MedFC (Frontal Medial Cortex)	43 voxels covering 7% of atlas.Ver45 (Vermis 4 5)
175 voxels covering 18% of atlas.MedFC (Frontal Medial Cortex)	195 voxels covering 15% of atlas.PaCiG l (Paracingulate Gyrus Left)	41 voxels covering 4% of atlas.pITG r (Inferior Temporal Gyrus, posterior division Right)
165 voxels covering 13% of atlas.PaCiG l (Paracingulate Gyrus Left)	189 voxels covering 7% of atlas.MidFG r (Middle Frontal Gyrus Right)	34 voxels covering 3% of atlas.Thalamus r
149 voxels covering 7% of atlas.Cereb8 r (Cerebelum 8 Right)	141 voxels covering 11% of atlas.pSMG r (Supramarginal Gyrus, posterior division Right)	33 voxels covering 8% of atlas.pPaHC l (Parahippocampal Gyrus, posterior division Left)
137 voxels covering 5% of atlas.MidFG r (Middle Frontal Gyrus Right)	106 voxels covering 7% of atlas.SPL r (Superior Parietal Lobule Right)	32 voxels covering 13% of atlas.Ver8 (Vermis 8)
108 voxels covering 9% of atlas.pSMG r (Supramarginal Gyrus, posterior division Right)	101 voxels covering 7% of atlas.SPL l (Superior Parietal Lobule Left)	31 voxels covering 10% of atlas.Pallidum l
80 voxels covering 5% of atlas.SPL r (Superior Parietal Lobule Right)	90 voxels covering 9% of atlas.AG l (Angular Gyrus Left)	31 voxels covering 4% of atlas.Hippocampus r
* T(190)_min = 3.34 ; k_min = 4	** T(190)_min = 3.13 ; k_min = 6	*** T(190)_min = 3.13 ; k_min = 6

Table 4: Analysis 1A: results and relative statistics. In the right column are reported results when the two-sided contrast was adopted, in the middle column those derived by the adoption of one-sided positive contrast, and on the left column those derived by the adoption of one-sided negative contrast. On the top of the table the 20 biggest clusters identified by the analysis are reported: their peak-voxel location within each cluster on the MNI space (Clusters x,y,z), their size, and the relative statistics are reported. On the bottom of the table the main belonging groups of all the suprathreshold voxels identified in the analysis are reported. Size-p-FWE = cluster-size p-value corrected for Family-Wise Error; size-p-FDR = cluster-size p-value corrected for False Discovery Rate; size p-unc = cluster-size p-value uncorrected; peak p-FWE = peak-voxel p-value corrected for Family Wise Error; peak p-unc = peak-voxel p-value uncorrected; T(190)_min = minimum T value; k_min = minimum number of voxels [27]. Complete data are reported in Supplemental material - Table 4B.

Analysis 1B

Clusters - two sided contrast*

Cluster number	Clusters - x,y,z	size	size p-FWE	size p-FDR	size p-unc	peak p-FWE	peak p-unc
1	+00 +22 +60	15	0.009627	0.007172	0.000023	1	0.000046
2	+00 +46 +38	13	0.025247	0.00948	0.000061	0.616786	0.000003
3	+12 -12 +18	9	0.190407	0.039153	0.0005	1	0.00006
4	-06 +06 +02	9	0.190407	0.039153	0.0005	0.999999	0.000013
-	-	-	-	-	-	-	-

All Suprathreshold voxels

5 voxels covering 0% of atlas.SFG r (Superior Frontal Gyrus Right)
4 voxels covering 0% of atlas.SFG l (Superior Frontal Gyrus Left)
3 voxels covering 0% of atlas.Thalamus r
2 voxels covering 0% of atlas.Thalamus l
1 voxels covering 0% of atlas.Caudate r
-
-
-
* T(190)_min = 3.34; k_min = 9

Clusters - positive contrast**

Cluster number	Clusters - x,y,z	size	size p-FWE	size p-FDR	size p-unc	peak p-FWE	peak p-unc
1	+64 -04 -02	17	0.013185	0.009197	0.000038	0.220127	0.000001
-	-	-	-	-	-	-	-
-	-	-	-	-	-	-	-
-	-	-	-	-	-	-	-
-	-	-	-	-	-	-	-

All suprathreshold voxels

10 voxels covering 4% of atlas.aSTG r (Superior Temporal Gyrus, anterior division Right)
7 voxels covering 0% of atlas.not-labeled
-
-
-
-
-
-
** T(190)_min = 3.13; k_min = 17

Clusters - negative contrast***

Cluster number	Clusters x,y,z	size	size p-FWE	size p-FDR	size p-unc	peak p-FWE	peak p-unc
1	+00 +22 +60	27	0.000336	0.000292	0.000001	1	0.000023
2	-12 +02 +20	18	0.0089	0.003882	0.000026	0.482303	0.000002
3	+00 +46 +38	16	0.019663	0.005748	0.000057	0.308393	0.000001
4	+12 -12 +18	14	0.044618	0.009909	0.000131	1	0.00003
5	-06 +06 +02	13	0.067819	0.012197	0.000202	0.998852	0.000007

All suprathreshold voxels

13 voxels covering 2% of atlas.Caudate l
11 voxels covering 0% of atlas.SFG r (Superior Frontal Gyrus Right)
5 voxels covering 0% of atlas.SFG l (Superior Frontal Gyrus Left)
4 voxels covering 1% of atlas.Caudate r
3 voxels covering 0% of atlas.Thalamus r
3 voxels covering 0% of atlas.Thalamus l
1 voxels covering 0% of atlas.PaCiG l (Paracingulate Gyrus Left)
48 voxels covering 0% of atlas.not-labeled
*** T(190)_min = 3.13 ; k_min = 13

*Table 5: Analysis 1B: results and relative statistics. In the right column are reported results when the two-sided contrast was adopted, in the middle column those derived by the adoption of one-sided positive contrast, and on the left column those derived by the adoption of one-sided negative contrast. On the top of the table the clusters identified by the analysis are reported: their peak-voxel location within each cluster on the MNI space (Clusters x,y,z), their size, and the relative statistics are reported. On the bottom of the table the belonging groups of all the suprathreshold voxels identified in the analysis are reported. Size-p-FWE = cluster-size p-value corrected for Family-Wise Error; size-p-FDR = cluster-size p-value corrected for False Discovery Rate; size p-unc = cluster-size p-value uncorrected; peak p-FWE = peak-voxel p-value corrected for Family Wise Error; peak p-unc = peak-voxel p-value uncorrected; T(190)_min = minimum T value; k_min = minimum number of voxels (*Chumbley et al., 2010*).*

Analysis 2A

Degree

ROI	bet	T	dof	p-unc	p-FDR
network	0.2	2E+15	190	< 0.000001	-
PreCG l	0.36	10.82	190	< 0.000001	< 0.000001
PreCG r	0.34	10.56	190	< 0.000001	< 0.000001
IC r	0.28	10.09	190	< 0.000001	< 0.000001
CO l	0.29	9.91	190	< 0.000001	< 0.000001
LG r	0.3	9.91	190	< 0.000001	< 0.000001
LG l	0.31	9.49	190	< 0.000001	< 0.000001
IC l	0.26	9.43	190	< 0.000001	< 0.000001
pMTG r	0.26	9.27	190	< 0.000001	< 0.000001
FP r	0.26	9.23	190	< 0.000001	< 0.000001
pMTG l	0.27	9.17	190	< 0.000001	< 0.000001
Cereb2 l	0.26	9.09	190	< 0.000001	< 0.000001
AG r	0.27	8.92	190	< 0.000001	< 0.000001
pSMG l	0.25	8.84	190	< 0.000001	< 0.000001
MidFG r	0.24	8.74	190	< 0.000001	< 0.000001
OP l	0.26	8.7	190	< 0.000001	< 0.000001
CO r	0.24	8.59	190	< 0.000001	< 0.000001
PostCG l	0.29	8.45	190	< 0.000001	< 0.000001

Average path length

ROI	bet	T	dof	p-unc	p-FDR
network	0.02	84.08	190	< 0.000001	-
pMTG r	0.02	39.84	190	< 0.000001	< 0.000001
pMTG l	0.02	37.88	190	< 0.000001	< 0.000001
FP r	0.02	37.09	190	< 0.000001	< 0.000001
AG l	0.02	37.03	190	< 0.000001	< 0.000001
MidFG l	0.02	37	190	< 0.000001	< 0.000001
IC r	0.02	36.01	190	< 0.000001	< 0.000001
IC l	0.02	35.97	190	< 0.000001	< 0.000001
FOrb l	0.02	35.94	190	< 0.000001	< 0.000001
SFG l	0.02	35.78	190	< 0.000001	< 0.000001
TP r	0.02	35.7	190	< 0.000001	< 0.000001
FP l	0.02	34.82	190	< 0.000001	< 0.000001
MidFG r	0.02	34	190	< 0.000001	< 0.000001
AG r	0.02	33.6	190	< 0.000001	< 0.000001
PO r	0.02	32.98	190	< 0.000001	< 0.000001
CO r	0.02	32.51	190	< 0.000001	< 0.000001
TP l	0.02	32.49	190	< 0.000001	< 0.000001
PreCG r	0.02	32.38	190	< 0.000001	< 0.000001

Clustering coefficient

ROI	beta	T	dof	p-unc	p-FDR
network	0.01	35.15	190	< 0.000001	-
pMTG l	0.01	16.83	190	< 0.000001	< 0.000001
pMTG r	< 0.01	15.69	190	< 0.000001	< 0.000001
FP l	0.01	15.44	190	< 0.000001	< 0.000001
IC l	< 0.01	14.95	190	< 0.000001	< 0.000001
FP r	< 0.01	14.74	190	< 0.000001	< 0.000001
FOrb l	< 0.01	14.69	190	< 0.000001	< 0.000001
AG l	< 0.01	14.42	190	< 0.000001	< 0.000001
CO r	0.01	14.35	190	< 0.000001	< 0.000001
PT l	0.01	14.31	190	< 0.000001	< 0.000001
PO r	0.01	14.25	190	< 0.000001	< 0.000001
MedFC	< 0.01	14.15	190	< 0.000001	< 0.000001
Cereb1 r	0.01	14.13	190	< 0.000001	< 0.000001
PT r	0.01	14.08	190	< 0.000001	< 0.000001
SFG l	0.01	14.06	190	< 0.000001	< 0.000001
IC r	< 0.01	13.72	190	< 0.000001	< 0.000001
PostCG r	0.01	13.69	189	< 0.000001	< 0.000001
Cereb2 r	< 0.01	13.66	188	< 0.000001	< 0.000001

Global efficiency

R	b	T	d	p-unc	p-FDR
n	0.	6	1	< 0.000001	-
p	0.	3	1	< 0.000001	< 0.000001
F	0.	3	1	< 0.000001	< 0.000001
IC	0.	3	1	< 0.000001	< 0.000001
Pr	0.	3	1	< 0.000001	< 0.000001
IC	0.	3	1	< 0.000001	< 0.000001
p	0.	3	1	< 0.000001	< 0.000001
Pr	0.	3	1	< 0.000001	< 0.000001
L	0.	3	1	< 0.000001	< 0.000001
M	0.	3	1	< 0.000001	< 0.000001
A	0.	3	1	< 0.000001	< 0.000001
C	0.	3	1	< 0.000001	< 0.000001
A	0.	3	1	< 0.000001	< 0.000001
M	0.	3	1	< 0.000001	< 0.000001
C	0.	3	1	< 0.000001	< 0.000001
F	0.	3	1	< 0.000001	< 0.000001
L	0.	3	1	< 0.000001	< 0.000001
F	0.	3	1	< 0.000001	< 0.000001

Local efficiency

ROI	beta	T	dof	p-unc	p-FDR
network	0.01	65.79	190	< 0.000001	-
pMTG l	0.01	42.03	190	< 0.000001	< 0.000001
pMTG r	0.01	37.14	190	< 0.000001	< 0.000001
IC l	0.01	37.1	190	< 0.000001	< 0.000001
PreCG r	0.01	36	190	< 0.000001	< 0.000001
IC r	0.01	34.98	190	< 0.000001	< 0.000001
CO r	0.01	34.96	190	< 0.000001	< 0.000001
PT l	0.01	34.54	190	< 0.000001	< 0.000001
AG l	0.01	34.38	190	< 0.000001	< 0.000001
PostCG r	0.01	33.82	189	< 0.000001	< 0.000001
LG r	0.01	33.14	190	< 0.000001	< 0.000001
aMTG r	0.01	32.62	190	< 0.000001	< 0.000001
PT r	0.01	31.89	190	< 0.000001	< 0.000001
CO l	0.01	31.87	190	< 0.000001	< 0.000001
FOrb l	0.01	30.43	190	< 0.000001	< 0.000001
MidFG r	0.01	30.4	190	< 0.000001	< 0.000001
aMTG l	0.01	30.15	190	< 0.000001	< 0.000001
FP l	0.01	29.74	190	< 0.000001	< 0.000001

Betweenness centrality

ROI	beta	T	dof	p-unc	p-FDR
network	< 0.01	46.1	190	< 0.000001	-
sLOC l	< 0.01	6.06	190	< 0.000001	0.000001
PreCG l	< 0.01	5.56	190	< 0.000001	0.000006
Cereb9 l	< 0.01	5.44	190	< 0.000001	0.000007
IC r	< 0.01	5.35	190	< 0.000001	0.000007
PP r	< 0.01	5.33	190	< 0.000001	0.000007
IFG oper l	< 0.01	5.28	190	< 0.000001	0.000007
pMTG r	< 0.01	5.26	190	< 0.000001	0.000007
PreCG r	< 0.01	5.21	190	< 0.000001	0.000008
Cereb6 l	< 0.01	5.08	190	0.000001	0.000013
SPL l	< 0.01	5.01	190	0.000001	0.000017
CO l	< 0.01	4.88	190	0.000002	0.000027
AG l	< 0.01	4.74	190	0.000004	0.000047
TP r	< 0.01	4.62	190	0.000007	0.00007
Cereb9 r	< 0.01	4.61	190	0.000007	0.00007
FP r	< 0.01	4.59	190	0.000008	0.00007
pPaHC r	< 0.01	4.58	190	0.000009	0.00007
Brain-Stem	< 0.01	4.54	190	0.00001	0.000077

iLOC r	0.28	8.37	190	< 0.000001	< 0.000001	Cereb2 l	0.02	32.16	190	< 0.000001	< 0.000001	aMTG r	< 0.01	13.5	190	< 0.000001	< 0.000001	T	0.	3	1	< 0.000001	< 0.000001	PO r	0.01	29.27	190	< 0.000001	< 0.000001	Cereb6 r	< 0.01	4.48	190	0.000013	0.000096
PP r	0.26	8.31	190	< 0.000001	< 0.000001	pSMG l	0.02	32.13	190	< 0.000001	< 0.000001	PreCG r	< 0.01	13.41	190	< 0.000001	< 0.000001	p	0.	3	1	< 0.000001	< 0.000001	LG l	0.01	29.25	190	< 0.000001	< 0.000001	MedFC	< 0.01	4.46	190	0.000014	0.000098

Table 6: Analysis 2A: results exposed using the graph theory and relative statistics. Degree, average oath length, clustering coefficient, global efficiency, local efficiency and betweenness centrality of the single ROIs are reported: for every one of these parameters, the twenty regions with the highest T-value are reported. ROI = Region of Interest; beta = beta value; T = T-value; dof = degree of freedom; p-unc = p-value uncorrected; p-FDR = p-value corrected for False Discovery Rate; FP r = Frontal Pole Right; FP l = Frontal Pole Left; IC r = Insular Cortex Right; IC l = Insular Cortex Left; SFG l = Superior Frontal Gyrus Left; MidFG r = Middle Frontal Gyrus Right; MidFG l = Middle Frontal Gyrus Left; IFG oper l = Inferior Frontal Gyrus, pars opercularis Left; PreCG r = Precentral Gyrus Right; PreCG l = Precentral Gyrus Left; TP r = Temporal Pole Right; TP l = Temporal Pole Left; aMTG r = Middle Temporal Gyrus, anterior division Right; aMTG l = Middle Temporal Gyrus, anterior division Left; pMTG r = Middle Temporal Gyrus, posterior division Right; pMTG l = Middle Temporal Gyrus, posterior division Left; PostCG r = Postcentral Gyrus Right; PostCG l = Postcentral Gyrus Left; SPL l = Superior Parietal Lobule Left; pSMG l = Supramarginal Gyrus, posterior division Left; AG r = Angular Gyrus Right; AG l = Angular Gyrus Left; sLOC l = Lateral Occipital Cortex, superior division Left; iLOC r = Lateral Occipital Cortex, inferior division Right; MedFC = Frontal Medial Cortex; FOrb l = Frontal Orbital Cortex Left; aPaHC r = Parahippocampal Gyrus, anterior division Right; LG r = Lingual Gyrus Right; LG l = Lingual Gyrus Left; CO r = Central Opercular Cortex Right; CO l = Central Opercular Cortex Left; PO r = Parietal Operculum Cortex Right; PP r = Planum Polare Right; PT r = Planum Temporale Right; PT l = Planum Temporale Left; OP l = Occipital Pole Left; Brain-Stem = Brain Stem; Cereb1 r = Cerebelum Crus1 Right; Cereb2 l = Cerebelum Crus2 Left; Cereb2 r = Cerebelum Crus2 Right; Cereb6 l = Cerebelum 6 Left; Cereb6 r = Cerebelum 6 Right; Cereb9 l = Cerebelum 9 Left; Cereb9 r = Cerebelum 9 Right. Complete data are reported in Supplemental material - Table 6B.

Analysis 2B

Degree						Average path length						Clustering coefficient						Global efficiency						Local efficiency						Bertweenness centrality					
ROI	beta	T	dof	p-unc	p-FDR	ROI	bet	T	dof	p-unc	p-FDR	ROI	bet	T	dof	p-unc	p-FDR	ROI	beta	T	dof	p-unc	p-FDR	ROI	bet	T	dof	p-unc	p-FDR	ROI	beta	T	dof	p-unc	p
network	< 0.01	238625657117635.1	190	< 0.000001	-	network	0.02	9.3	190	< 0.000001	-	network	0.01	4.4	190	0.000018	-	network	< 0.01	6.93	190	< 0.000001	-	network	0.01	7.86	190	< 0.000001	-	network	< 0.01	2.68	190	0.008027	-
aPaHC r	0.01	3.85	190	0.000162	0.021372	PreCG l	0.03	6.15	190	< 0.000001	0.000001	aITG r	0.02	4.06	185	0.000074	0.009737	TP l	0.01	5.58	190	< 0.000001	0.000007	AG l	0.01	5.71	190	< 0.000001	0.000006	-	-	-	-	-	-
-	-	-	-	-	-	IC r	0.02	5.28	190	< 0.000001	0.000023	PP r	0.01	3.72	190	0.000265	0.017481	SFG l	0.01	5.47	190	< 0.000001	0.000007	IC r	0.01	5.37	190	< 0.000001	0.00001	-	-	-	-	-	-
-	-	-	-	-	-	PreCG r	0.02	4.96	190	0.000002	0.000068	sLOC l	0.01	3.42	190	0.000772	0.033952	FP l	0.01	5.41	190	< 0.000001	0.000007	PreCG r	0.01	5.37	190	< 0.000001	0.00001	-	-	-	-	-	-
-	-	-	-	-	-	Ver6	0.04	4.74	187	0.000004	0.000125	-	-	-	-	-	-	pMTG r	0.01	5.36	190	< 0.000001	0.000007	pMTG l	0.01	5.19	190	0.000001	0.000016	-	-	-	-	-	-
-	-	-	-	-	-	Ver45	0.05	4.71	188	0.000005	0.000125	-	-	-	-	-	-	TP r	0.01	5.32	190	< 0.000001	0.000007	PT l	0.01	5.17	190	0.000001	0.000016	-	-	-	-	-	-
-	-	-	-	-	-	IC l	0.02	4.53	190	0.00001	0.000227	-	-	-	-	-	-	pMTG l	0.01	5.29	190	< 0.000001	0.000007	IC l	0.01	5.07	190	0.000001	0.000021	-	-	-	-	-	-
-	-	-	-	-	-	Cereb9 l	0.05	4.48	186	0.000013	0.000248	-	-	-	-	-	-	PaCiG l	0.01	5.21	190	< 0.000001	0.000009	PostCG r	0.01	5.01	189	0.000001	0.000023	-	-	-	-	-	-
-	-	-	-	-	-	IFG tri l	0.03	4.38	190	0.00002	0.000292	-	-	-	-	-	-	PO r	0.01	5	190	0.000001	0.000022	CO l	0.01	4.96	190	0.000002	0.000025	-	-	-	-	-	-
-	-	-	-	-	-	FOrb r	0.02	4.38	190	0.00002	0.000292	-	-	-	-	-	-	FOrb l	0.01	4.94	190	0.000002	0.000024	aMTG l	0.01	4.91	190	0.000002	0.000028	-	-	-	-	-	-
-	-	-	-	-	-	OP l	0.03	4.35	190	0.000022	0.000293	-	-	-	-	-	-	CO r	0.01	4.8	190	0.000003	0.000039	CO r	0.01	4.86	190	0.000002	0.000032	-	-	-	-	-	-
-	-	-	-	-	-	IFG oper l	0.03	4.31	190	0.000027	0.000319	-	-	-	-	-	-	MidFG l	0.01	4.79	190	0.000003	0.000039	pMTG r	0.01	4.8	190	0.000003	0.000039	-	-	-	-	-	-
-	-	-	-	-	-	Cereb9 r	0.06	4.26	188	0.000033	0.000347	-	-	-	-	-	-	AG l	0.01	4.77	190	0.000004	0.000039	aMTG r	0.01	4.67	190	0.000006	0.000056	-	-	-	-	-	-
-	-	-	-	-	-	Cereb7 r	0.04	4.25	182	0.000034	0.000347	-	-	-	-	-	-	MedFC	0.01	4.73	190	0.000004	0.000045	TP l	0.01	4.67	190	0.000006	0.000056	-	-	-	-	-	-
-	-	-	-	-	-	CO l	0.02	4.18	190	0.000044	0.000397	-	-	-	-	-	-	SCC l	0.01	4.65	190	0.000006	0.000057	PP r	0.01	4.66	190	0.000006	0.000056	-	-	-	-	-	-
-	-	-	-	-	-	SMA r	0.02	4.18	190	0.000045	0.000397	-	-	-	-	-	-	Precuneous	0.01	4.64	190	0.000007	0.000057	PT r	0.01	4.62	190	0.000007	0.000061	-	-	-	-	-	-
-	-	-	-	-	-	Cereb2 l	0.02	4.16	190	0.000049	0.000404	-	-	-	-	-	-	tolTG r	0.01	4.58	190	0.000008	0.000068	LG l	0.01	4.51	190	0.000011	0.000092	-	-	-	-	-	-

-	-	-	-	-	-	AG r	0.02	4.1	190	0.00006	0.000468	-	-	-	-	-	-	FP r	0.01	4.42	190	0.000017	0.000128	sLOC l	0.01	4.32	190	0.000025	0.000191	-	-	-	-	-	-
-	-	-	-	-	-	Cereb7 l	0.04	4.06	187	0.000071	0.000523	-	-	-	-	-	-	aMTG r	0.01	4.41	190	0.000017	0.000128	MidFG r	0.01	4.26	190	0.000032	0.000233	-	-	-	-	-	-
-	-	-	-	-	-	MidFG r	0.02	4.03	190	0.000079	0.000551	-	-	-	-	-	-	aMTG l	0.01	4.28	190	0.000029	0.000204	aITG r	0.02	4.22	185	0.000038	0.000261	-	-	-	-	-	-

Table 7: Analysis 2B: results exposed using the graph theory and relative statistics. Degree, average oath length, clustering coefficient, global efficiency, local efficiency and betweenness centrality of the single ROIs are reported: for global efficiency, local efficiency and average path length, the twenty regions with the highest T-value are reported. ROI = Region of Interest; beta = beta value; T = T-value; dof = degree of freedom; p-unc = p-value uncorrected; p-FDR = p-value corrected for False Discovery Rate; FP r = Frontal Pole Right; FP l = Frontal Pole Left; IC r = Insular Cortex Right; IC l = Insular Cortex Left; SFG l = Superior Frontal Gyrus Left; MidFG r = Middle Frontal Gyrus Right; MidFG l = Middle Frontal Gyrus Left; IFG oper l = Inferior Frontal Gyrus, pars opercularis Left; PreCG r = Precentral Gyrus Right; PreCG l = Precentral Gyrus Left; TP r = Temporal Pole Right; TP l = Temporal Pole Left; aMTG r = Middle Temporal Gyrus, anterior division Right; aMTG l = Middle Temporal Gyrus, anterior division Left; pMTG r = Middle Temporal Gyrus, posterior division Right; pMTG l = Middle Temporal Gyrus, posterior division Left; aITG r = Inferior Temporal Gyrus, anterior division Right; toITG r = Inferior Temporal Gyrus, temporooccipital part Right; PostCG r = Postcentral Gyrus Right; AG r = Angular Gyrus Right; AG l = Angular Gyrus Left; sLOC l = Lateral Occipital Cortex, superior division Left; MedFC = Frontal Medial Cortex; SMA r = Juxtapositional Lobule Cortex -formerly Supplementary Motor Cortex- Right; PaCiG l = Paracingulate Gyrus Left; Precuneous = Precuneous Cortex; FOrb l = Frontal Orbital Cortex Left; aPaHC r = Parahippocampal Gyrus, anterior division Right; LG l = Lingual Gyrus Left; CO r = Central Opercular Cortex Right; CO l = Central Opercular Cortex Left; PO r = Parietal Operculum Cortex Right; PP r = Planum Polare Right; PT r = Planum Temporale Right; PT l = Planum Temporale Left; SCC l = Supracalcarine Cortex Left; Cereb2 l = Cerebelum Crus2 Left; Cereb7 r = Cerebelum 7b Right; Cereb9 l = Cerebelum 9 Left; Cereb9 r = Cerebelum 9 Right; Ver45 = Vermis 4 5; Ver6 = Vermis 6. Complete data are reported Supplemental material - Table 7B.

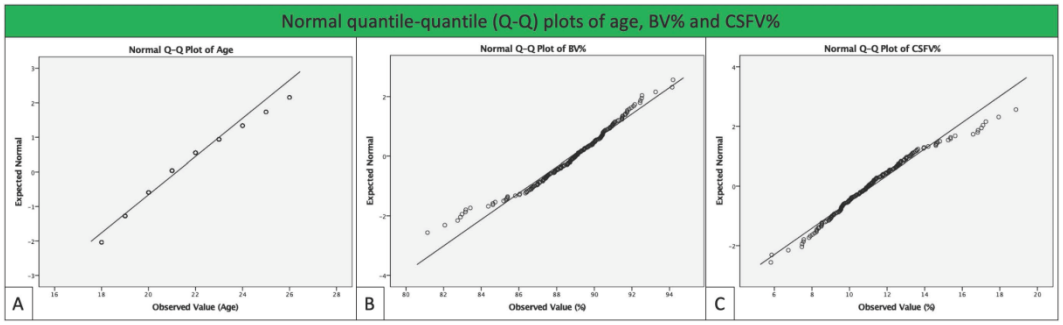

ejn_14627_f1.tiff

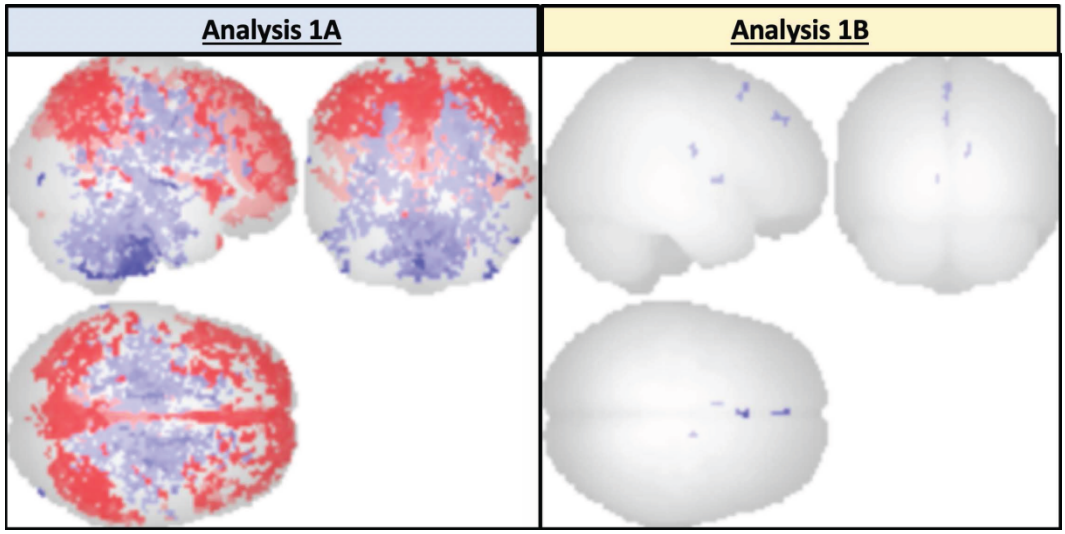

ejn_14627_f2.tiff

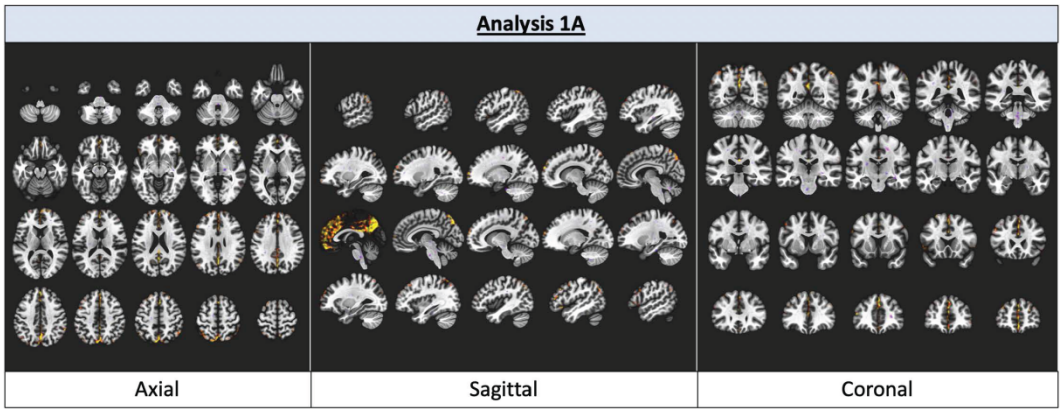

ejn_14627_f3.tiff

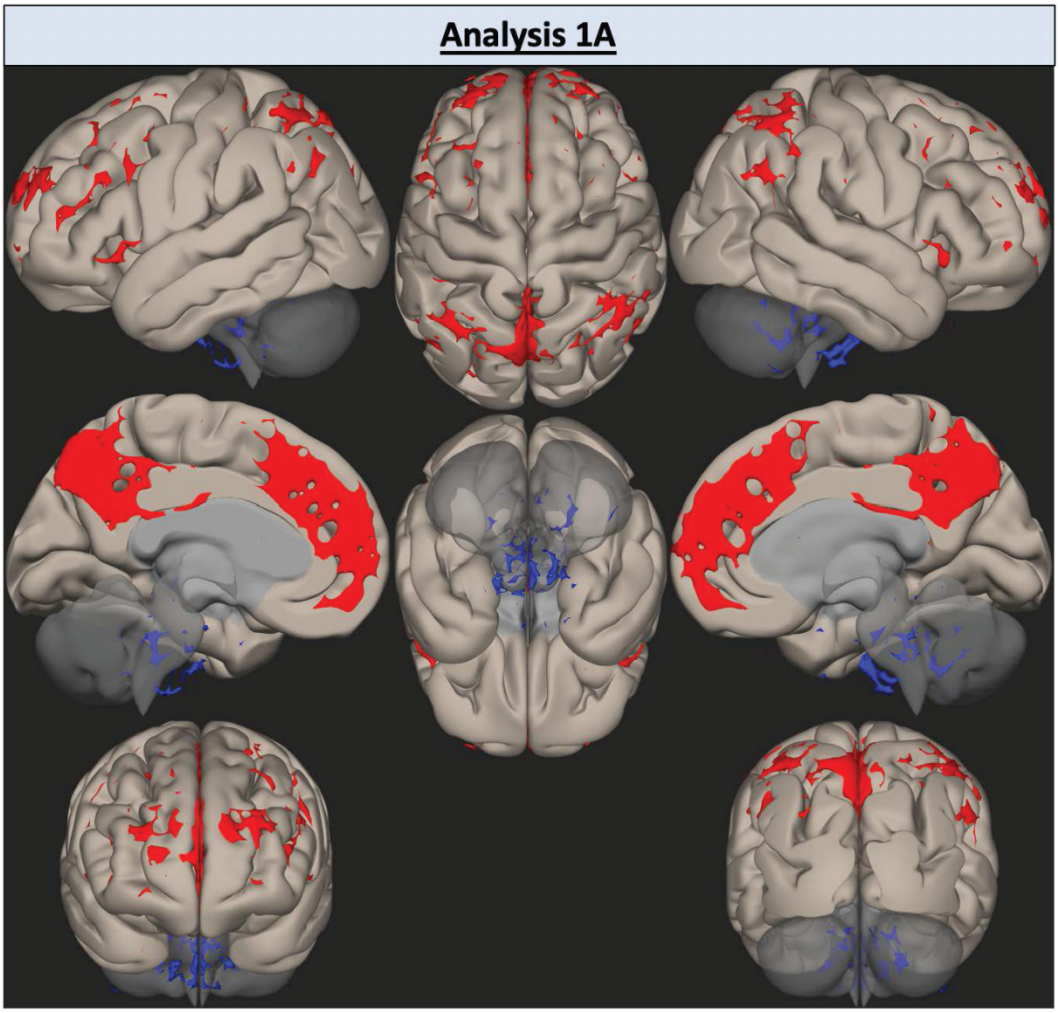

ejn_14627_f4.tiff

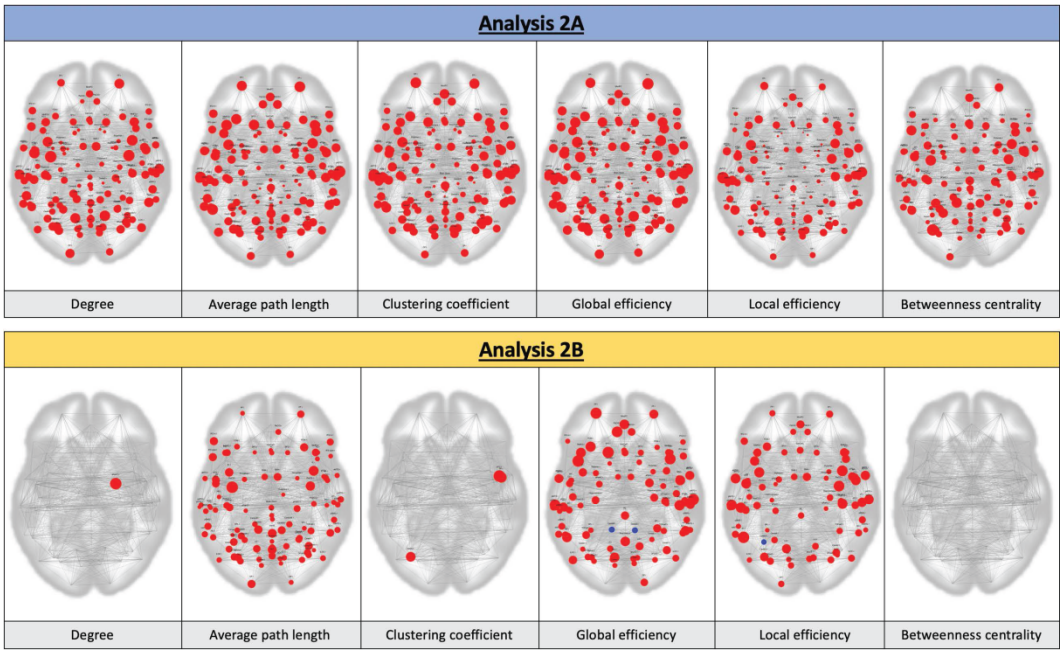

ejn_14627_f5.tiff